Title: **Modeling Insights into Potential Mechanisms of Opioid-Induced Respiratory Depression within Medullary and Pontine Networks**

Authors: Wendy L. Olsen[1,3*], John A. Hayes[1,2*], Dale Shuman[4], Kendall F. Morris[4], and Donald C. Bolser[1,2]

Author affiliations:

[1]Breathing Research and Therapeutics (BREATHE) Center, University of Florida, Gainesville, FL

[2]Department of Physiological Sciences, University of Florida, Gainesville, FL

[3]Department of Rehabilitation Sciences, Appalachian State University, Boone NC

[4]Department of Molecular Pharmacology and Physiology, University of South Florida, Tampa, FL

* contributed equally

ORCIDs:

Wendy L. Olsen ORCID: 0000-0002-7607-8096

John A. Hayes ORCID: 0000-0003-2849-7672

Kendall F. Morris ORCID: 0000-0001-6582-1203

Donald C. Bolser ORCID: 0000-0002-4577-8954

Corresponding author: olsenwl@appstate.edu

Keywords: OIRD**,** opioids, glutamate release, fentanyl, mu-opioid receptors, mu-OR, μ-OR, modeling, preBötzinger Complex, pons, medulla

Funding: Supported by NIH 1R01HL155721-01, 1R01HL163008, and T32HL134621.

Table of Contents Category: Computational Physiology and Modelling

Author contributions: Conception or design of the work: W.L.O. and D.C.B. Acquisition, analysis or interpretation of data for the work: W.L.O. and J.A.H. Drafting the work or revising it critically for important intellectual content: W.L.O., J.A.H., D.S., K.F.M., and D.C.B. All authors have read and approved the final version of this manuscript and agree to be accountable for all aspects of the work in ensuring that questions related to the accuracy or integrity of any part of the work are appropriately investigated and resolved.

Running title: Mechanisms of Mammalian Opioid-Induced Respiratory Depression

ABSTRACT (246 of 250 words)

The opioid epidemic is a pervasive health issue and continues to have a drastic impact on the United States. This is primarily because opioids cause respiratory suppression and the leading cause of death in opioid overdose is respiratory failure (*i.e.*, opioid-induced respiratory depression, OIRD). Opioid administration can affect the frequency and magnitude of inspiratory motor drive by activating μ-opioid receptors that are located throughout the respiratory control network in the brainstem. This can significantly affect ventilation and blunt CO_2 responsiveness, but the precise neural mechanisms that suppress breathing are not fully understood. Previous research has suggested that opioids affect medullary and pontine inspiratory neuron activity by disrupting upstream elements within this circuit. Inspiratory neurons within this network exhibit synchrony consistent with shared excitation from other neuron populations and recurrent mechanisms. One possible target for opioid suppression of inspiratory drive are excitatory synapses. Reduced excitability of these synaptic elements may result in disfacilitation and reduced synchrony among inspiratory neurons. Downstream effects of disfacilitation may result in abnormal output from phrenic motoneurons resulting in distressed breathing. We tested the plausibility of this hypothesis with a computational model of the respiratory network by targeting the synaptic excitability in fictive medullary and pontine populations. The synaptic conductances were systematically decreased while monitoring the overall respiratory motor pattern and aggregate firing rates of subsets of cell populations. Simulations suggest that highly selective, rather than generalized, actions of opioids on synapses within the inspiratory network may account for different observed breathing mechanics.

INTRODUCTION

Opioids are considered the gold standard for the treatment of chronic and acute pain, when used appropriately. This is especially true in a perioperative and postoperative environment (Hill and Canals 2022; Palkovic et al. 2020). The risks associated with opioid use follow a dose-dependent response and has ensured that their availability remain restricted (Bateman et al. 2021; Hill and Canals 2022; Mattson et al. 2021). However, the opioid epidemic remains a clear and increasingly pervasive health crisis in the United States (Ramirez et al. 2021). In 2019, overdose deaths increased by more than 50.6% since 2013 (Mattson et al. 2021). This increase is largely attributed to the illicit distribution and use of fentanyl. The primary cause of death in opioid overdose is respiratory depression (Hill and Canals 2022; Ramirez et al. 2021). Thus, research has been dedicated to uncovering the mechanisms associated with opioid-induced respiratory-depression (OIRD) and uncovering neural pathways to reverse OIRD (Bateman et al. 2021; Ramirez et al. 2021).

Breathing

Multiple regions within the brain and brainstem can contribute to OIRD (Bateman et al. 2021; Lalley 2003; Ramirez et al. 2021). The brainstem is the primary hub that holds afferent and efferent neurons that drive breathing and breathing-related behaviors. These neurons work together to form connections that regulate respiration in mammals (Lindsey et al. 2012). These circuits control the drive to breathe, cardiorespiratory functioning, and maintain ventilation (Segers et al. 2015). Rhythmic respiratory activity is facilitated and modified by interactions between the bilaterally distributed respiratory control network located within the ventrolateral medulla (Baekey et al. 2004) and certain regions within the pons (Levitt et al. 2015; Varga et al. 2019). This interconnectedness of medullary and pontine neurons is essential for breathing (Lindsey et al. 2012).

The preBötzinger complex (preBötC), located within the medulla, has been reported to generate a coupled respiratory rhythm with the parafacial/retrotrapezoid regions (Bochorishvili et al. 2012; Mellen et al. 2003; Pattinson 2008). The parafacial/retrotrapezoid nuclei are involved in active expiration and central chemoreception. The Bötzinger complex maintains neurons that are active during expiration and is a major source of inhibition (Bateman et al. 2021; Varga et al. 2019), and these processes contribute to pacing respiration (Bateman et al. 2021). Inspiratory bursts generated by the preBötC network determine breathing frequency (Burgraff et al. 2021). Neurons experience a gradual increase in excitation that synchronizes to produce a coordinated population burst (Baertsch et al. 2019). Synaptic connections within the medulla coordinate these population bursts via excitatory and inhibitory networks to facilitate rhythmogenesis (Baertsch et al. 2019; Burgraff et al. 2021; Ramirez et al. 2021). Studies perturbing the preBötC with opioids, in particular, have reported apnea (Wenninger et al. 2004),

respiratory failure (Wenninger et al. 2004), and deficits in airway protection (Shen et al. 2022). For example, in a series of studies conducted by Lalley and colleagues oscillation and burst patterns of respiratory rhythm are slowed and decreased by doses of fentanyl (Lalley 2003; Lalley and Mifflin 2017).

The ventrolateral medulla is not the only region participating in respiratory rhythm generation. Areas of the rostral pontine circuitry, that include the Kölliker-Fuse nucleus, the parabrachial complex, and the locus coeruleus, also contribute to rhythmogenesis by delivering dense excitatory feedback to the respiratory control network in the ventrolateral medulla (Pattinson 2008), stabilizing the respiratory rate, and generating eupneic breathing patterns (Levitt et al. 2015; Varga et al. 2019). Researchers found that these specific sites (*i.e.*, the Kölliker-Fuse nucleus, the parabrachial complex, and the locus coeruleus) contribute to the generation of the three-phase normal, eupneic respiratory pattern: inspiration, post-inspiration, and active expiration (Abdala et al. 2009). Additionally, the medulla receives sensory information from the pontine network that affects respiration. Specifically, the nucleus tractus solitarius receives afferent feedback from peripheral sites (*i.e.*, pulmonary stretch receptors, bronchopulmonary C-fibers, and chemosensory information from carotid and aortic bodies) (Bateman et al. 2021). Studies perturbing the pontine nuclei resulted in respiratory rate alterations (Bonis et al. 2010), ventilatory changes (Abdala et al. 2009), and tidal volume changes (Levitt et al. 2015). Contributions from the pons and medullary areas form a spatially dynamic network that produces and controls respiratory rhythm (Abdala et al. 2009; Baertsch et al. 2019; Segers et al. 2015).

Opioids and the Respiratory Control Network

Opioids alter breathing by activating μ-opioid receptors (μ-ORs) throughout the brainstem (Dahan et al. 2010). Pharmacological effects and adverse events are mediated by the presence of μ-ORs that are found at multiple sites within the central and peripheral nervous system (Varga et al. 2019). In the ventrolateral medulla, the preBötzinger complex is active during inspiration and has been found to be extremely sensitive to opioid agonists (Pattinson 2008). Previous research has studied these effects within intact animals and medullary slices. Results indicated that opioids have presynaptic and postsynaptic effects that alter the excitability of brainstem respiratory neurons (Gray et al. 1999, 2001). Lalley further investigated the effects of systemic administration of fentanyl by measuring intracellular membrane potentials of respiratory bulbospinal, vagal, and propriobulbar neurons in anesthetized and unanesthetized decerebrate cats (Lalley 2003). Lalley concluded that fentanyl had effects presynaptic to respiratory motoneurons to depress neuronal activity. Additional rodent studies observed discrete, rather than continual, stepwise depression in phrenic output and inspiratory neuron discharges by opioids. These results are attributed to the effects on circuits upstream to inspiratory neurons within the

preBötzinger complex (Janczewski and Feldman 2006; Mellen et al. 2003). For example, applying the opioid agonist DAMGO to the Kölliker-Fuse nucleus causes robust apneusis in a working heart–brainstem preparation of rat (Levitt et al. 2015). However, how opioid agonists fully affect inspiratory neurons within the respiratory control network remains unclear. What has been implicated across several studies is that ventrolateral medullary and pontine circuitry, together, are affected by opioid administration and this in turn affects respiration (Burgraff et al. 2021; Dahan et al. 2010; Janczewski and Feldman 2006; Lalley 2003; Mellen et al. 2003).

The most common adverse effect of opioid use reported is respiratory depression, which in the extreme can directly lead to death (Pattinson 2008). Previous researchers have used intracellular recordings to measure membrane potentials of inspiratory neurons to better understand the inhibitory effects within the respiratory control network (Gray et al. 1999, 2001; Lalley 2003; Lalley and Mifflin 2017; Mellen et al. 2003). Local application of opioid agonists affects the somatodendritic μ-ORs on spatially confined presynaptic terminals while receptors in the broader region are left unaffected. This phenomenon can be difficult to interpret when the pontine and medullary circuitry, specifically the preBötzinger complex and the Kölliker-Fuse nucleus, reciprocally share sensory-motor information to generate inspiratory bursts and respiratory patterns (Varga et al. 2019). Recently, Chou and coworkers (Chou et al. 2024) disseminated findings from a computational model that described plausible explanations for the observed variations in experimental responses to opioids. The group explains that their model accounts for the fixed and dynamic excitatory/inhibitory μ-OR+ neurons, cellular parameters, and network connections. They attribute discrete assigned randomness to these parameters within the model that influence individual nodes. This small level of difference is sufficient to introduce enough variance to explain the variances in experimental preparations. However, understanding the neural network connections and respiratory mechanisms that are affected by opioids is of widespread interest to researchers.

A joint neural-biomechanical computational model

Lalley and coworkers (Lalley 2003; Lalley and Mifflin 2017) have interpreted their results of suppressed breathing and disfacilitation of discharge patterns as an attenuation of presynaptic excitability within the pontomedullary circuitry. We have tested the plausibility of this hypothesis with a joint-neuromechanical model of the respiratory network (Lindsey et al. 2012; O'Connor et al. 2012). This model uses an integrate-and-fire neural network that drives deterministic equations that simulate human respiratory mechanics (O'Connor et al. 2012). The first aim of the current study was to systematically and individually decrease the strength of medullary inspiratory neuron connections within this joint neural-biomechanical model to examine the overall respiratory output. The second aim was to systematically,

and individually, decrease the strength of pontine neuron connections within the same model. Model and trial specifications are described in the Materials and Methods section.

MATERIALS AND METHODS

Network simulations

A joint neural biomechanical model (Lindsey et al. 2012; O'Connor et al. 2012), was applied to test the hypothesis that decreasing the synaptic conductance of medullary and pontine inspiratory neurons induces opioid-mediated respiratory breathing patterns. The neural components of the model were derived from previously described respiratory network models of discrete integrate-and-fire neurons after MacGregor (MacGregor 1987) and a hybridized bursting integrate-and-fire population based on Hodgkin-Huxley equations (Breen et al. 2003). The latter was previously developed from a continuously integrated model (Butera et al. 1999). The current model was derived from these equations paired with *in vivo* data that enhanced the development. Ultimately, motor output from phrenic populations at each time step (0.5 ms) within the model are calculated by counting the total spikes from all the cells in each of two phrenic populations ($P0$ and $P1$) and dividing by the duration of a time step. Each population accounts for different inspiratory burst activity within the medullary component of the model. The output of the two can best be described by the equation:

$$\frac{0.3 \cdot P0 + 0.7 \cdot P1}{200}$$

Notably, there should be a maximum value of 1 for phrenic population recruitment. This equation describes the model's representation of inspiratory output. The lumbar motor output is handled in a similar way as the phrenic output with two lumbar motoneuronal populations ($L0$ and $L1$):

$$\frac{0.3 \cdot L0 + 0.7 \cdot L1}{80}$$

The biomechanical components of the model (Lindsey et al. 2012; O'Connor et al. 2012) were developed from transdiaphragmatic pressure and diaphragm activation while controlling the thoracoabdominal configuration (Cluzel et al. 2000; Grassino et al. 1978; Konno and Mead 1967; Song et al. 2006).

The *uflsim* software package, version 1.0.36 (Lindsey et al. 2012; O'Connor et al. 2012) utilizes a *Qt C*++ cross-platform development framework written for Windows and Linux (source code may be found here: https://github.com/jahayes-ns/uflsim with Windows binaries here: https://github.com/jahayes-ns/uflsim/releases/download/neuroscience/uflsim_win_1.0.36.zip).

The program includes the functionality of the program *SYSTM11* (MacGregor 1987) used in previous simulations of the respiratory network. The program allows neuron excitability to be modulated

by injected current, and elements designated as “fiber populations” external to the network can also be used to represent transiently active afferent inputs to the network. A graphical user interface (*simbuild*) was used to modify cell parameters and network structure while the resulting model files were simulated using *simrun*. Simulations were run on 64-bit Intel-based computers under the Windows or Linux operating systems. Python scripts were developed to produce large sets of *uflsim* networks (.snd files) with varied parameters such as synaptic strengths between populations of neurons, so simulations could be executed in batches and analyzed offline with figures produced using *Matplotlib* (Hunter 2007). Network summary figures (Figs. 3D-E, 5, 6B-C, 8B-C, and 9B-C) were produced by taking the mean±SEM of relevant features from 9 distinct runs of freshly produced networks derived from a “trunk” network (Fig. 2). These 9 distinct networks were randomly generated with different random seed values.

Neuron simulations

Single-cell neuron simulations of the Butera model (Butera et al. 1999) were performed using *XPPAUT* (Ermentrout 2002). Parameter values were taken from the original study except for the changes described in Results. Panels for the figures were produced using *Matplotlib* (Hunter 2007) and *pandas* (team 2024).

RESULTS

Organization of a fictive bulbar and spinal respiratory network

We started with the network structure from a previously published respiratory model (O’Connor et al. 2012). This is comprised of 47 populations of neurons with up to 70-300 members each (9159 total neurons) as well as 10 fiber sources that project to these neuronal populations (1800 total fibers). Each population member had 50-200 axon terminals randomly distributed to members of its target populations (average source→target were 100.1 terminals for each pair) with 175,394,850 total terminals in the network. The identity of the neurons in each population are defined by three characteristics: 1) their typical firing phenotype under eupneic conditions, 2) their general anatomical location, and 3) their hypothesized, or experimentally identified, connectivity to other populations in the model (Fig. 1). Typically, the prefix of the eupneic inspiratory-phasing neurons are “I-” and eupneic expiratory-phasing neurons with “E-”. After this “Aug”, “Dec”, suggests the predominant discharge pattern during the respective phase as augmenting or decrementing spike rate consistent with experimental phenotypes. “NRM” indicates that a population is not eupneic respiratory modulated. Anatomical locations for the populations are sometimes specified parenthetically with “pons” or “raphe” and the remainder are by default in the medulla. The exception to the latter is the “PHRENIC” and

223 “LUMBAR” populations of motoneurons and are meant to represent roughly the C4 and L1 levels of the
224 spinal cord and output to muscles.
225 Figure 1A highlights 17 of the key populations from this model network in the context of the
226 present study with gray boxes generally delineating the approximate anatomical location (pons,
227 medulla, and spinal cord) for the firing phenotypes. Figure 1B shows hypothesized lateral connections
228 within these structures, while Figure 1C and 1D show ascending and descending connections between
229 these structures, respectively.
230 Figure 2 shows the population activity of each of these populations where the core respiratory
231 rhythm-generating circuit is shown in Fig. 2A. Medullary interneurons (INs) periodically oscillate
232 bursting between the inspiratory (I) and expiratory phases (E) with the I-Driver neurons initiating the
233 cycles, I-Dec neurons following a similar firing pattern, and I-Aug neurons reciprocally inhibiting the
234 others. These medullary neurons project to bulbospinal premotoneurons that further project to cervical
235 motoneurons (Phrenic MNs) and lower spinal cord (Lumbar MNs) (Fig. 2B). Our biomechanical model
236 accounts for the activity from these MNs, as well as laryngeal MNs (not shown), to model airway
237 mechanics that drive lung inflation/deflation (Fig. 2C). Pulmonary stretch receptors (PSRs) then both
238 excite I-Aug and inhibit I-Dec neurons during inflation closing a feedback loop (Fig. 2D).
239
240 *The relationship of I-Driver cellular properties to fictive breathing*
241 The I-Driver neurons form the core kernel of the rhythm generator that produce the initial burst activity
242 that percolates through the inspiratory phase (Fig. 2A). A sub-spike threshold, slowly-inactivating
243 “persistent” sodium current (I_{NaP}) produces this augmenting activity during the late-expiratory phase
244 and is described by the following equation (modified from (Breen et al. 2003)):
250 $$I_{NaP}(V_m) = \bar{g}_{NaP} \cdot m_\infty(V_m) \cdot h_{NaP} \cdot (V_m - E_{Na})$$
245 Figure 3 illustrates the subthreshold activity of this I_{NaP} current. Fig. 3A shows the membrane voltage
246 trajectory (V_m) of an intrinsically bursting I-Driver-like neuron with the inactivation variable (h_{NaP}) in the
247 middle row and the I_{NaP} truncated to -50 pA in the bottom row to highlight the slowly de-inactivating
248 current between bursts of activity. E_{Na} is the Nernst reversal potential for sodium (+50 mV) while
249 $m_\infty(V_m)$ is the instantaneous voltage-dependent activation function for I_{NaP}.
251 Figure 3B shows the same simulated neuron with the maximum synaptic conductance ($\bar{g}_{NaP}$)
252 slightly decreased to a scaling factor of 95% (0.95x) which slows the bursting frequency. Further
253 decreasing the scaling factor to 90% (0.9x) resulted in a silent neuron that relaxes to a subthreshold
254 baseline V_m (not shown). In the same simulated neuron, returning to the original $\bar{g}_{NaP}$ but changing the
255 maximum time constant of NaP inactivation ($\tau_{h\text{-}NaP}$) to 50% (0.5x) results in a dramatic increase in the
256 bursting frequency in Fig. 3C.

For comparison to the more expansive network model, similar graded adjustments on 300 I-Driver neurons from scaling factors 1.0x to 0.0x to $\bar{g}_{NaP}$ and $\tau_{h\text{-}NaP}$ led to changes in T_i (inspiratory phase duration), T_e (expiratory phase duration), and T_{tot} (the sum of T_i and T_e, or full cycle period) and is shown in Fig. 3D. Similar to the neuron model, changing $\bar{g}_{NaP}$ led to cessation of rhythm at relatively high levels of scaling factor for $\bar{g}_{NaP}$ suggesting the importance of subthreshold I_{NaP} in this model to initiate the population burst activity. Remarkably, in contrast to the single neuron model, decreasing $\tau_{h\text{-}NaP}$ increased both the expiratory phase (inter-burst interval) and consequently the full cycle period (T_{tot}) while having only a modest effect on T_i. This qualitatively shows the dramatic impact network connectivity and synaptic properties can have on the overall production of rhythmic behavior in this model brainstem, and we explore this in more detail below.

Generalized mechanisms for μ-OR-agonist influence on the neural control of respiration

In this study, we analyzed several distinct schemes by which μ-OR agonists may influence respiratory activity (Fig. 4). The first are comprised of cellular effects that are conceptualized as affecting baseline membrane properties through K^+-dominated leak channels and will be examined more closely associated with Fig. 5. The key take-away from this mechanism is that, in the absence of active membrane properties more dramatic than spike-generating currents, it would simply affect the presynaptic spike rates of neurons and can be simulated by an adjustment in applied stimulus current (I_{app}) (Fig. 4A). In contrast, mechanisms that influence connectivity strength could act through pre- or postsynaptic mechanisms (Fig. 4B) and will be considered in the subsequent Results sections (Fig. 6-10). For the purposes of this study, they are effectively the same mechanism and result in decreased I_{syn} (synaptic current) given a uniform spike-rate between the two.

μ-OR agonists have been shown to directly cause Fig. 4A.iii and Fig. 4B.ii in some contexts (Gray et al. 1999; Heinke et al. 2011; Ikoma et al. 2007; Jørgensen et al. 2022; Kim et al. 2024) and Fig. 4B.i may be one mechanism of opioid tolerance (Gillis et al. 2020; Koch and Höllt 2008).

Alteration of excitability in populations of the upstream core network

We first started by examining the effects of biasing cellular excitability by altering I_{app} over the range -10 to +10 pA, where the latter depolarizes neurons. There were 4 conditions, changes in ΔI_{app} on the populations of: I-Drivers, I-Drivers + I-Augs, NRM-pons, and all neurons in the simulation for comparison. The results are analogous to the situations demonstrated in Fig. 4Ai-iii.

There were 9 distinct runs of independently generated starting networks ($\Delta I_{app} = 0$) for the 4 conditions. Changing $\Delta I_{app} > 0$ for all neurons slows the respiratory rhythm (T_{tot}) as $\Delta I_{app} >> 0$ but also slows the rhythm slightly as inspiratory phase bursts (T_i) increase when $\Delta I_{app} < 0$ (Fig. 5A). If $\Delta I_{app} < 0$

291 falls too low the system loses respiratory activity. As this ceases at ΔI_{app} < ~-2 pA across all networks it
292 shows that the current system is very "stiff" and just on the precipice of cessation if the whole network is
293 seriously perturbed in the hyperpolarizing direction.
294 For I-Driver + I-Aug perturbations, there is a transient period as $\Delta I_{\text{app}} < 0$ where the CV of T_{tot}, T_i,
295 and T_e, increase dramatically compared to similar I-Driver perturbations (Fig. 5A). Curiously, when I-
296 Driver population alone is manipulated the means of both T_i and T_e roughly track along the same
297 trajectories as I-Driver + I-Aug perturbations. This shows that the I-Aug population is contributing to
298 cycle-to-cycle stability of the respiratory rhythm.
299 We also modulated NRM-pons neurons to see how they influence overall respiratory activity.
300 While they are non-phasic, the stochasticity of this population's firing still influences activity in non-
301 intuitive, non-monotonic ways as a function of uniform ΔI_{app} (Fig. 5A). At $\Delta I_{\text{app}} > 0$, breathing became
302 deeper, and lungs are inflated while at $\Delta I_{\text{app}} < 0$ breaths are shallower (Fig. 5B). Similar trends were
303 found in the more targeted perturbations of I-Drivers and I-Drivers + I-Augs suggesting the NRM-pons
304 neurons are vicariously acting largely through these populations as the connectivity from NRM-pons
305 implies (Fig. 1D).
306
307 *Intraplanar medullary synaptic sources affect rhythm generation*
308 The essential elements of the respiratory network are found in the medullary region, so we examined
309 how modulating the maximal excitatory strength ($\bar{g}_{Excit}$) between planar connections in this structure
310 could influence activity (Fig. 6).
311 Fig. 6A illustrates the subset of anatomically (hypothesized) planar medullary connections from
312 Fig. 1A and 1B and we were focused on the role of excitatory connections. We scaled down the
313 synaptic strength (analogous to Fig. 4B) between the following populations of neurons: I-Drivers → I-
314 Drivers, I-Drivers → I-Augs, I-Drivers → I-Decs, I-Drivers → I-Drivers/I-Augs/I-Decs, and I-Augs → I-
315 Augs (Fig. 6A).
316 Scaling the strength of recurrent synapses in the I-Driver population (I-Drivers → I-Drivers)
317 resulted in relatively little change in T_{tot}, T_i, or T_e (Fig. 6B). Further, perturbation of the strength of these
318 recurrent synapses had little effect on phrenic amplitude, lung volume or peak inspiratory flow (Fig. 6C).
319 Reducing synaptic strength between the I-Driver and I-Aug populations increased T_{tot} by over
320 15% and that effect was primarily due to an increase in T_e of over 30% (Fig. 6B). There was little effect
321 on T_i by this perturbation. Further, there were linear reductions in both phrenic amplitude, lung volume,
322 and peak inspiratory flow (Fig. 6C). Figure 7A shows the spike-time histogram patterns of setting the
323 synaptic strength from I-Driver to I-Aug neurons to 0%. The Phrenic MNs lose robust temporal
324 coherence which explains the reduction in Flow and Lung Volume (compare to Fig. 2).

When synaptic strength between the I-Driver and I-Dec populations was reduced, rhythmogenesis and inspiratory motor drive failed after a change between 60-80% (Fig. 6B, C). Figs. 7B and C show examples of firing rate records for medullary and bulbospinal neurons as well as phrenic and abdominal motoneurons during reduction of synaptic strength to 80% (Fig. 7B), and 60% (Fig. 7C) of control for I-Driver to I-Dec synapses.

Simultaneous reductions in the synaptic strength from I-Drivers to other I-Driver neurons, I-Aug neurons and I-Dec neurons resulted in what appeared to be a synthesis of all changes induced by perturbation of excitability for each of the individual populations alone (Fig. 6B, C). As such, simultaneous reductions in synaptic strength by up to 55% increased T_{tot} and T_e and decreased phrenic amplitude, lung volume and peak inspiratory flow (Fig. 6B, C). Large reductions in synaptic strength resulted in simulated apnea.

We additionally decreased synaptic strength among recurrent synapses in the I-Aug population alone. Unlike perturbation of synaptic strength among recurrent synapses within the I-Driver population; this action lengthened both T_{tot} and T_i by 15-25% with no change in T_e (Fig. 6B). Further, phrenic amplitude, lung volume, and peak inspiratory flow were also reduced in a linear manner (Fig. 6C).

Inhibitory influence of I-Dec hub neurons

Since the I-Dec population of neurons seems to have a dramatic effect on respiratory activity, we decided to also examine the effects of the I-Dec synaptic connections (Fig. 8). This is novel in comparison to the previous figures in that we were probing the influence of inhibitory synapses.

Perturbing all the inhibitory connections from the I-Dec population (Fig. 8A) causes the respiratory behavior to drop (Fig. 8B/C) because these neurons are the hub of our system with connections to 19 of the other 46 populations of neurons (10 inhibitory connections shown). In general, as the maximal inhibitory strength ($\bar{g}_{Inhib}$) decrease the T_i, T_e, and T_{tot} get shorter and these quantities get more regular (Fig. 8B), and the phrenic activity monotonically increases (Fig. 8C). When $\bar{g}_{Inhib}$ is 60% of control, Fig.8D demonstrates hyperpnea-like activity with intense inspiratory/expiratory activity and large lung inflations/deflations before the rhythm goes out in Fig. 8E when $\bar{g}_{Inhib}$ drops to 55% and lower.

Descending pontine synaptic sources affect burst patterning

Finally, we also looked at how perturbing $\bar{g}_{Excit}$ between NRM and I-Aug or I-Driver neurons affected the overall breathing pattern. Decreasing the excitatory connections from the pontine synaptic sources (Fig. 9A) led to disordered and inconsistent T_i, T_e, and $T_{tot.}$ production (Fig 9B). When $\bar{g}_{Excit}$ is blocked, phrenic activity does increase for the I-Aug + I-Driver and I-Driver connections. However, it decreases

for the I-Aug connections and remains unchanged for the I-pons connections (Fig 9C). Blocking this descending pontine transmission led to clustered breathing (Fig. 10).

DISCUSSION

The effects of opioids on respiratory function in experimental conditions is variable. In fact, little is known about the variance of in-between subjects' effects of opioid use (Dunn et al. 2019, 2020). The current study investigated the simulated responses of an opioid within a computational model of the pontomedullary respiratory network to better understand the neural mechanisms contributing to OIRD.

The opioid epidemic remains a critical research priority. There are many effects that opioids pose on respiratory function in experimental and clinical conditions (e.g., decreases or abnormal function in chest wall compliance, tidal volume, respiratory rate, etc.). This has led to much investigation that has focused on the impact of different opioid agonists on the upper airway in respiratory depression (Skulsky et al. 2007). However, respiratory depression is a common deleterious feature of opioid use. The current study investigated the simulated responses of activating μ-ORs within a computational model of the pontomedullary respiratory network to better understand the neural mechanisms contributing to OIRD. Since morphine, codeine, and similar drugs, have multiple side effects beyond just activating μ-ORs (Dahan 2007; Simera et al. 2010; Tomazini Martins et al. 2018), our model is best interpreted to most closely reproduce the highly specific μ-OR ligand fentanyl (Lalley 2003; Shen et al. 2022).

Simulated opioid effects on respiratory activity

To model these opioid effects, we decreased the synaptic strength across medullary neurons associated with rhythmogenesis. Previous computational models have perturbed the connection probabilities (Chou et al. 2024), time constants of central and peripheral chemoreceptors (Magosso et al. 2004), and the polarization of sodium channels (Shevtsova et al. 2011) to assess the effects of opioids on respiration specifically within fictive medullary neurons. The advantage of the current study, with the employed joint neural network-biomechanical model, is that we examined these factors at a biomechanical level and in the context of a broader brainstem neuronal network.

Overall, the strength of the network's connectivity is an important parameter that affects the neural breathing patterns, and the model is generally inhibited when perturbed by opioids. While decreasing the connection strength or explicitly hyperpolarizing member populations, breathing patterns were significantly affected. OIRD is characterized by a decrease in respiratory rate and irregular breathing frequencies and at high doses apnea. This has been attributed to opioids activating G-

coupled proteins through μ-ORs which hyperpolarize cells through G-protein-gated inward rectifying K^+ (GIRK) channels (Montandon et al. 2016a, 2016b).

Previous *in vivo* studies have reported decreased respiratory rates when opioids were directly applied to the ventrolateral medulla or systemically injected (Montandon et al. 2016b, 2016a). For example, when DAMGO (d-Ala2, *N*-MePhe4, Gly-ol]-enkephalin), was applied to the ventrolateral medulla and presumably activating local μ-ORs, it reduced the respiratory rate of mice, but did not affect the diaphragm amplitude in GIRK2$^{-/-}$ mice (Montandon 2022). In the same study, a moderate intramuscular injection of fentanyl was provided to the GIRK2$^{-/-}$ mice, and only a slight depression in diaphragm amplitude was observed. In a complementary study, systemic administration of fentanyl reportedly decreased respiratory rate, yet had no effect on diaphragm amplitude (Montandon et al. 2016a, 2016b).

The administration of opioids has been shown to affect the burst duration of respiratory motor units up to the point of respiratory arrest (Lalley 2006). As discussed above, one mechanism opioids likely perturb respiratory patterns is through cell hyperpolarization, which in turn, affects the spiking activity of respiratory neurons (Fig. 4A). In our simulations, modulating an injected bias current (I_{app}) within the core medullary populations (Fig. 5) affected spike burst durations (T_i) until the respiratory activity was extinguished at larger hyperpolarizing I_{app}. Therefore, within our modeling efforts, modifying the injected current qualitatively reproduces *in vivo* effects of OIRD.

Lalley (2003) investigated the intravenous effects of fentanyl in adult cats while recording individual neurons. He reported prolonged discharges that induced tonic firing of bulbospinal expiratory neurons (like our E-Aug-BS population) that were correlated with a reduced hyperpolarization of synaptic drive potentials. Lalley suggested that this result may have been explained by the decrease in the duration of the inspiratory phase observed at certain dose-responses of fentanyl (Lalley 2003). He further interpreted lower doses of fentanyl to have a similar effect on vagal post-inspiratory motoneurons which led to “sparse, low-frequency” discharges which suggests that fentanyl regulates bulbospinal and motoneurons presynaptically at different dose-dependent responses (Lalley 2003; Lalley and Mifflin 2017) similar to a combination of Fig. 4Aiii and Fig. 4Bii.

Fictive respiratory rhythm generation and patterning

An important consideration for this model is that the I-Driver population are fundamentally essential for any kind of respiratory patterning under our simulated conditions. All members of that population burst based on a slowly-inactivating persistent sodium current (I_{NaP}) (Breen et al. 2003; Butera et al. 1999) which has been recently shown to be inessential for I-Driver-like activity (da Silva et al. 2023). For this

study, there is no salient difference in what bursting mechanism we choose for the I-Driver population as we are interested in network effects as emphasized by the depiction in Fig. 3.

However, considering our model when $\bar{g}_{NaP}$ was altered, this led to the cessation of the network rhythm (Fig. 3D). Essentially by decreasing I_{NaP} the cells broadly hyperpolarize, and the network aborted the respiratory rhythm. However, as we showed in Figure 3, modulating the parameters determining the qualities of $\bar{g}_{NaP}$ on individual I-Driver neurons has a dichotomous effect versus how the more expansive multi-population network behaves.

This is consistent with previous findings: Phillips and Baertsch reported when lowering [K^+] within their model (which hyperpolarizes neurons) it mimicked *in vitro* experiments by increasing the presence of weaker "burstlet" rhythms (Phillips and Baertsch 2024). This is hypothesized to be driven by preinspiratory spiking as opposed to intrinsic bursting within the network. Further, Baertsch and coworkers (Baertsch et al. 2021) earlier reported that ventrolateral medullary excitatory postsynaptic potential amplitudes were reduced in the presence of opioids, specifically by DAMGO, and that μ-OR activation suppresses excitatory synapses from the preBötC neurons to their post-synaptic targets. Thus, reducing excitability within the respiratory network (Del Negro et al. 2005).

Respiratory efforts and breathing are finely tuned and well-timed behaviors. They must be executed with precision to prevent maladaptive consequences. These behaviors are primarily regulated by the nucleus tractus solitarius and the ventral respiratory column. The presence of opioids has been reported to adversely affect the coordination and execution of these crucial behaviors. The speed of the network was altered when we manipulated $\tau_{h\text{-}NaP}$ in the I-Driver population which also affected burst duration. Similar results have been reported by Baertsch and colleagues (Baertsch et al. 2021). These motor unit spiking behaviors can be divided into three phases: refractory, percolation, and burst phases. Researchers have reported that when fentanyl is administered, a neuron's discharge identity is altered, causing changes in timing and frequency (Baertsch et al. 2021; Lalley and Mifflin 2017). Changes in frequency and neuron identities are modulated by opioid membrane activity. Opioid activity, within the ventral respiratory column, causes asynchronous activity, and, depending on the opioid agonist, can cause varying effects on motoneurons. For example, Baertsch and Ramirez (Baertsch et al. 2019) reported that substance P affected the percolation phase, also referred to as the recurrent excitation phase, of the inspiratory rhythm by increasing the pre-inspiratory neurons' rate of firing by activating a depolarizing current (Hayes and Del Negro 2007). Researchers have reported that when fentanyl is administered, a neuron's discharge identity is altered, causing changes in timing and frequency. Lalley and Mifflin (Lalley and Mifflin 2017) postulated that μ-opioid agonists directly affect the controlling and timing of burst and oscillation patterns of bulbospinal and vagal motoneurons, which also have a direct effect on respiratory muscle force. Specifically, they reported that a threshold dose (3

μg/kg) of intravenous fentanyl had an increase in burst frequencies, oscillation intensities, and a more negative action potential threshold that had a direct effect on overall breathing pattern.

Physiological implications

One of the motivations for this kind of modeling study is that experimental studies of this kind are currently unfeasible. Here, we are delineating neuronal populations of interest both anatomically and, more importantly, functionally, because the respiratory network is distributed across much of the brainstem (Segers et al. 2008). With advancing genetic technologies these avenues may be more closely explored but challenges remain and may require higher-order intersectional approaches than what is currently common.

In the case of anatomical specificity, approaches such as viral injections into specific locations can partially address these issues (Liu et al. 2021; Varga et al. 2020). Especially, when expression from these injections may be conditioned on specific gene promoters (Nectow and Nestler 2020). However, specifying genetic tools to firing pattern is especially nebulous for the most part. A combination of ion channel expression, endogenous Ca^{2+} buffers such as parvalbumin (Alheid et al. 2002), synaptic partners, or constitutively expressed transcription factors (Bachmutsky et al. 2020; Sun et al. 2019), may provide a means of intersectionally subdividing certain populations given a certain neuronal population's "fingerprint" of multiple distinguishing criteria but that remains beyond the scope of the present study.

It is important to note that several μ-opioid agonists have been investigated and reported varying effects (Burgraff et al. 2023; Danaf et al. 2023; Hiranita et al. 2024; Neumueller et al. 2023). For example, Burgraff, Baertsch, and Ramirez (2023) reported the effects of morphine and fentanyl on breathing and airway stability. Specifically, the administration of fentanyl resulted in the disruption of airflow that were resolved with a tracheostomy and/or the administration of salbutamol and adrenaline. These airflow obstructions were absent during the administration of morphine (Burgraff et al. 2023). Similar effects have been reported in emergency departments and within other hospital settings (e.g., perioperative and postoperative conditions) (Sutter et al. 2015; Wolf et al. 2020).

Opioids are clinically used for their analgesic effects perioperatively and postoperatively. However, their use can lead to respiratory depression and the disfacilitation of airway protective mechanisms. The early detection of respiratory suppression allows clinicians to make life-saving decisions and avert the catastrophic consequences of OIRD. The overall results of our modeling efforts indicate that the joint neural-biomechanical model employed in the current study demonstrated overall inhibition, frequency alterations, spike burst changes, and timing changes, which are broadly supported by the different perturbations observed in *in vivo* data that employs the μ-OR agonist fentanyl. The

proposed model is an excellent tool that lends itself to answering questions that persist within the opioid crisis, specifically revolving around OIRD.

FIGURE LEGENDS

Figure 1. Connectivity among key elements of the model network. A, The core neuronal populations interrogated in this study. Orange inverted arrow connections represent excitatory connections while blue solid circle connections represent inhibitory connections. The graph is arranged roughly corresponding to hypothesized anatomical location with top-tier rostral pontine populations, middle-tier medullary populations, and spinal cord populations representing the motoneuronal output of the neuronal network at the bottom tier. **B-D**, the planar (**B**), ascending (**C**), and descending (**D**) subsets of these connections to improve clarity.

Figure 2. Fictive eupnea with active expiration. A, The core respiratory time course of activity by classes of overlayed neuronal populations. The top are pontine interneurons (Pons INs), middle medullary interneurons (Medulla INs), and bottom medullary bulbospinal premotor neurons (Bulbospinal INs). **B**, Inspiratory motor output of the simulation as expressed as phrenic motoneuronal activity (Phrenic MNs) while lumbar spinal motoneurons (Lumbar MNs) convey expiratory activity. **C**, Simulated lung volume and flow at the mouth produced by the respiratory activity. **D**, Moving average of lung pulmonary stretch receptors (Lung PSRs) activated by lung expansion. This vagal sensory information feeds back into the core respiratory circuit continuously. Arrows indicate the feedforward flow of information in the system.

Figure 3. Comparison of I_{NaP} at the neuronal and network level. A, top, In a simple model of a single respiratory neuron, I_{NaP} can lead to periodic bursting in membrane potential (V_m). (middle), The magnitude and kinetics of I_{NaP} are controlled by the inactivation gating variable h_{NaP} (bottom). **B**, Decreasing $\bar{g}_{NaP}$ slows the burst frequency. **C**, Decreasing the rate h_{NaP} inactivates ($\tau_{h\text{-}NaP}$) increases the burst frequency. **D**, Effects on the full network period (T_{tot}), burst duration (T_i), and expiratory phase (T_e), when decreasing $\bar{g}_{NaP}$ and $\tau_{h\text{-}NaP}$ in the I-Driver population of neurons. CV is the coefficient of variation. **E**, The same effects on motoneuronal output and biomechanical respiratory flow.

Figure 4. High-level comparison of possible cellular and synaptic effects of μOR-agonists. Presynaptic neuronal (left spheres) spiking with neurotransmitter release (small circles) onto postsynaptic neurons (right spheres). Clear boxes on the postsynaptic neurons represent transmitter

receptors. **A**, i.), Normal presynaptic spiking activity is equivalent to normal synaptic strength (1.0x $\bar{g}_{syn}$) and $\Delta I_{\text{app}} = 0$. ii.), Heightened presynaptic spiking activity is equivalent to normal synaptic strength and $\Delta I_{\text{app}} > 0$. iii.), Lower presynaptic spiking activity is equivalent to normal synaptic strength and $\Delta I_{\text{app}} < 0$. **B**, i.), Normal presynaptic spiking activity with normal neurotransmitter release but fewer postsynaptic receptor targets is equivalent to $\Delta I_{\text{app}} = 0$ and <1.0x $\bar{g}_{syn}$ but weaker synaptic strength from a "postsynaptic effect". ii.), Normal presynaptic spiking activity with decrease in neurotransmitter release but normal receptor targets is also equivalent to $\Delta I_{\text{app}} = 0$ and <1.0x $\bar{g}_{syn}$ but weaker synaptic strength from a "presynaptic effect".

Figure 5. Influence of ΔI_{app} on network and biomechanical behaviors. A, T_{tot} is total respiratory period, T_i, inspiratory phase duration, and T_e, the expiratory phase duration. CV is the coefficient of variation for the respective quantities. **B**, (top) Maximum phrenic motoneuron amplitude during the inspiratory phase. (middle) Maximum lung volume during the inspiratory phase. (bottom) Inspiratory flow. ΔI_{app} is in units of pA.

Figure 6. Influence of excitatory synaptic strength on network and biomechanical behaviors through medullary planar connections. A, Illustration of the excitatory planar connections from Fig. 1B that are analyzed here. **B**, T_{tot} is respiratory period, T_i, inspiratory phase duration, and T_e, the expiratory phase duration. CV is the coefficient of variation for the respective quantities. **C**, (top) Maximum phrenic motoneuron amplitude during the inspiratory phase (arbitrary units) (middle) Maximum lung volume during the inspiratory phase. (bottom) Inspiratory flow.

Figure 7. Example activity patterns of key planar excitatory connection perturbations. A, Spike-time histogram patterns of the network with I-Driver output to I-Aug neurons at 0% of control. **B**, Spike-time histogram patterns of the network with I-Driver output to I-Dec neurons at 80% of control compared to 60% of control (**C**).

Figure 8. Influence of inhibitory synaptic strength on network and biomechanical behaviors through I-Dec hub connections. A, Illustration of the inhibitory connections from I-Dec neurons in Fig. 1A that are collectively altered here. **B**, T_{tot} is respiratory period, T_i, inspiratory phase duration, and T_e, the expiratory phase duration. CV is the coefficient of variation for the respective quantities. **C**, (top) Maximum phrenic motoneuron amplitude during the inspiratory phase (arbitrary units). (middle) Maximum lung volume during the inspiratory phase. (bottom) Inspiratory flow. **D**, The spike-time

histogram patterns of the network with I-Dec inhibitory output at 60% of control compared to 40% of control (**E**).

Figure 9. Influence of excitatory synaptic strength on network and biomechanical behaviors through descending pontine-medullary connections. A, Illustration of the descending excitatory connections from pontine non-respiratory modulated neurons (NRM-pons), phase spanning neurons (rIE-pons, cIE-pons, EI-pons), and inspiratory neurons (I-pons). **B**, T_{tot} is respiratory period, T_i, inspiratory phase duration, and T_e, the expiratory phase duration. CV is the coefficient of variation for the respective quantities. **C**, (top) Maximum phrenic motoneuron amplitude during the inspiratory phase (arbitrary units). (middle) Maximum lung volume during the inspiratory phase. (bottom) Inspiratory flow.

Figure 10. Example activity patterns of descending excitatory connection perturbations from NRM-pons neurons. The network pattern with NRM-pons excitatory output at 20% of control projecting to I-Aug and I-Driver populations resulting in clustered-like bursts in inspiratory activity.

574 ## REFERENCES

575 **Abdala APL**, **Rybak IA**, **Smith JC**, **Zoccal DB**, **Machado BH**, **St-John WM**, **Paton JFR**. Multiple pontomedullary
576 mechanisms of respiratory rhythmogenesis. *Respir Physiol Neurobiol* 168: 19–25, 2009.
577 **Alheid GF**, **Gray PA**, **Jiang MC**, **Feldman JL**, **McCrimmon DR**. Parvalbumin in respiratory neurons of the
578 ventrolateral medulla of the adult rat. *J Neurocytol* 31: 693–717, 2002.
579 **Bachmutsky I**, **Wei XP**, **Kish E**, **Yackle K**. Opioids depress breathing through two small brainstem sites. *eLife* 9:
580 e52694, 2020.
581 **Baekey DM**, **Morris KF**, **Nuding SC**, **Segers LS**, **Lindsey BG**, **Shannon R**. Ventrolateral medullary respiratory
582 network participation in the expiration reflex in the cat. *J Appl Physiol* 96: 2057–2072, 2004.
583 **Baertsch NA**, **Bush NE**, **Burgraff NJ**, **Ramirez J-M**. Dual mechanisms of opioid-induced respiratory depression in
584 the inspiratory rhythm-generating network. *eLife* 10: e67523, 2021.
585 **Baertsch NA**, **Severs LJ**, **Anderson TM**, **Ramirez J-M**. A spatially dynamic network underlies the generation of
586 inspiratory behaviors. *Proc Natl Acad Sci* 116: 7493–7502, 2019.
587 **Bateman JT**, **Saunders SE**, **Levitt ES**. Understanding and countering opioid-induced respiratory depression. *Br J*
588 *Pharmacol* bph.15580, 2021.
589 **Bochorishvili G**, **Stornetta RL**, **Coates MB**, **Guyenet PG**. Pre-Bötzinger complex receives glutamatergic
590 innervation from galaninergic and other retrotrapezoid nucleus neurons. *J Comp Neurol* 520: 1047–1061,
591 2012.
592 **Bonis JM**, **Neumueller SE**, **Krause KL**, **Kiner T**, **Smith A**, **Marshall BD**, **Qian B**, **Pan LG**, **Forster HV**. Site-specific
593 effects on respiratory rhythm and pattern of ibotenic acid injections in the pontine respiratory group of
594 goats. *J Appl Physiol* 109: 171–188, 2010.
595 **Breen BJ**, **Gerken WC**, **Butera RJ**. Hybrid Integrate-and-Fire Model of a Bursting Neuron. *Neural Comput* 15:
596 2843–2862, 2003.
597 **Burgraff NJ**, **Baertsch NA**, **Ramirez J-M**. A comparative examination of morphine and fentanyl: unravelling the
598 differential impacts on breathing and airway stability. *J Physiol* n/a, 2023.
599 **Burgraff NJ**, **Bush NE**, **Ramirez JM**, **Baertsch NA**. Dynamic Rhythmogenic Network States Drive Differential
600 Opioid Responses in the *In Vitro* Respiratory Network. *J Neurosci* 41: 9919–9931, 2021.
601 **Butera RJ**, **Rinzel J**, **Smith JC**. Models of respiratory rhythm generation in the pre-Bötzinger complex. I. Bursting
602 pacemaker neurons. *J Neurophysiol* 82: 382–397, 1999.
603 **Chou GM**, **Bush NE**, **Phillips RS**, **Baertsch NA**, **Harris KD**. Modeling Effects of Variable preBötzinger Complex
604 Network Topology and Cellular Properties on Opioid-Induced Respiratory Depression and Recovery.
605 *eNeuro* 11, 2024.
606 **Cluzel P**, **Similowski T**, **Chartrand-Lefebvre C**, **Zelter M**, **Derenne J-P**, **Grenier PA**. Diaphragm and Chest Wall:
607 Assessment of the Inspiratory Pump with MR Imaging—Preliminary Observations. *Radiology* 215: 574–583,
608 2000.
609 **Dahan A**. Novel data on opioid effect on breathing and analgesia. *Semin Anesth Perioper Med Pain* 26: 58–64,
610 2007.
611 **Dahan A**, **Aarts L**, **Smith TW**. Incidence, Reversal, and Prevention of Opioid-induced Respiratory Depression.
612 *Anesthesiology* 112: 226–238, 2010.
613 **Danaf J**, **da Silveira Scarpellini C**, **Montandon G**. βγ G-proteins, but not regulators of G-protein signaling 4,
614 modulate opioid-induced respiratory rate depression. *Front Physiol* 14, 2023.
615 **Del Negro CA**, **Morgado-Valle C**, **Hayes JA**, **Mackay DD**, **Pace RW**, **Crowder EA**, **Feldman JL**. Sodium and Calcium
616 Current-Mediated Pacemaker Neurons and Respiratory Rhythm Generation. *J Neurosci* 25: 446–453, 2005.
617 **Dunn KE**, **Barrett FS**, **Brands B**, **Marsh DC**, **Bigelow GE**. Individual differences in human opioid abuse potential as
618 observed in a human laboratory study. *Drug Alcohol Depend* 205: 107688, 2019.
619 **Dunn KE**, **Weerts EM**, **Huhn AS**, **Schroeder JR**, **Tompkins DA**, **Bigelow GE**, **Strain EC**. Preliminary evidence of
620 different and clinically meaningful opioid withdrawal phenotypes. *Addict Biol* 25: e12680, 2020.

621 **Ermentrout B**. *Simulating, Analyzing, and Animating Dynamical Systems: A Guide to XPPAUT for Researchers and*
622 *Students*. SIAM, 2002.
623 **Gillis A**, **Kliewer A**, **Kelly E**, **Henderson G**, **Christie MJ**, **Schulz S**, **Canals M**. Critical Assessment of G Protein-
624 Biased Agonism at the μ-Opioid Receptor. *Trends Pharmacol Sci* 41: 947–959, 2020.
625 **Grassino A**, **Goldman MD**, **Mead J**, **Sears TA**. Mechanics of the human diaphragm during voluntary contraction:
626 statics. *J Appl Physiol* 44: 829–839, 1978.
627 **Gray PA**, **Janczewski WA**, **Mellen N**, **McCrimmon DR**, **Feldman JL**. Normal breathing requires preBötzinger
628 complex neurokinin-1 receptor-expressing neurons. *Nat Neurosci* 4: 927–930, 2001.
629 **Gray PA**, **Rekling JC**, **Bocchiaro CM**, **Feldman JL**. Modulation of Respiratory Frequency by Peptidergic Input to
630 Rhythmogenic Neurons in the PreBötzinger Complex. *Science* 286: 1566–1568, 1999.
631 **Hayes JA**, **Del Negro CA**. Neurokinin Receptor-Expressing Pre-Bötzinger Complex Neurons in Neonatal Mice
632 Studied In Vitro. *J Neurophysiol* 97: 4215–4224, 2007.
633 **Heinke B**, **Gingl E**, **Sandkühler J**. Multiple Targets of μ-Opioid Receptor-Mediated Presynaptic Inhibition at
634 Primary Afferent Aδ- and C-Fibers. *J Neurosci* 31: 1313–1322, 2011.
635 **Hill R**, **Canals M**. Experimental considerations for the assessment of in vivo and in vitro opioid pharmacology.
636 *Pharmacol Ther* 230: 107961, 2022.
637 **Hiranita T**, **Ho NP**, **France CP**. Ventilatory Effects of Fentanyl, Heroin, and d-Methamphetamine, Alone and in
638 Mixtures in Male Rats Breathing Normal Air. *J Pharmacol Exp Ther* 388: 244–256, 2024.
639 **Hunter JD**. Matplotlib: A 2D Graphics Environment. *Comput Sci Eng* 9: 90–95, 2007.
640 **Ikoma M**, **Kohno T**, **Baba H**. Differential Presynaptic Effects of Opioid Agonists on Aδ- and C-afferent
641 Glutamatergic Transmission to the Spinal Dorsal Horn. *Anesthesiology* 107: 807–812, 2007.
642 **Janczewski WA**, **Feldman JL**. Distinct rhythm generators for inspiration and expiration in the juvenile rat:
643 Rhythm generators for inspiration and expiration. *J Physiol* 570: 407–420, 2006.
644 **Jørgensen AB**, **Rasmussen CM**, **Rekling JC**. μ-Opioid Receptor Activation Reduces Glutamate Release in the
645 PreBötzinger Complex in Organotypic Slice Cultures. *J Neurosci* 42: 8066–8077, 2022.
646 **Kim HR**, **Dey S**, **Sekerkova G**, **Martina M**. μ-Opioid Receptor Modulation of the Glutamatergic/GABAergic
647 Midbrain Inputs to the Mouse Dorsal Hippocampus. *J Neurosci* 44, 2024.
648 **Koch T**, **Höllt V**. Role of receptor internalization in opioid tolerance and dependence. *Pharmacol Ther* 117: 199–
649 206, 2008.
650 **Konno K**, **Mead J**. Measurement of the separate volume changes of rib cage and abdomen during breathing. *J*
651 *Appl Physiol* 22: 407–422, 1967.
652 **Lalley PM**. μ-Opioid receptor agonist effects on medullary respiratory neurons in the cat: evidence for
653 involvement in certain types of ventilatory disturbances. *Am J Physiol-Regul Integr Comp Physiol* 285:
654 R1287–R1304, 2003.
655 **Lalley PM**. Opiate slowing of feline respiratory rhythm and effects on putative medullary phase-regulating
656 neurons. *Am J Physiol-Regul Integr Comp Physiol* 290: R1387–R1396, 2006.
657 **Lalley PM**, **Mifflin SW**. Oscillation patterns are enhanced and firing threshold is lowered in medullary respiratory
658 neuron discharges by threshold doses of a μ-opioid receptor agonist. *Am J Physiol-Regul Integr Comp*
659 *Physiol* 312: R727–R738, 2017.
660 **Levitt ES**, **Abdala AP**, **Paton JFR**, **Bissonnette JM**, **Williams JT**. μ opioid receptor activation hyperpolarizes
661 respiratory-controlling Kolliker–Fuse neurons ¨ and suppresses post-inspiratory drive. *J Physiol Neurosci*
662 593: 4453–4469, 2015.
663 **Lindsey BG**, **Rybak IA**, **Smith JC**. Computational Models and Emergent Properties of Respiratory Neural
664 Networks. In: *Comprehensive Physiology*, edited by Terjung R. Wiley, p. 1619–1670.
665 **Liu S**, **Kim D-I**, **Oh TG**, **Pao GM**, **Kim J-H**, **Palmiter RD**, **Banghart MR**, **Lee K-F**, **Evans RM**, **Han S**. Neural basis of
666 opioid-induced respiratory depression and its rescue. *Proc Natl Acad Sci* 118: e2022134118, 2021.
667 **MacGregor RJ**. *Neural and Brain Modeling*. New York: Academic Press, 1987.

Magosso E, **Ursino M**, **vanOostrom JH**. Opioid-Induced Respiratory Depression: A Mathematical Model for Fentanyl. *IEEE Trans Biomed Eng* 51: 1115–1128, 2004.

Mattson CL, **Tanz LJ**, **Quinn K**, **Kariisa M**, **Patel P**, **Davis NL**. Trends and Geographic Patterns in Drug and Synthetic Opioid Overdose Deaths — United States, 2013–2019. *MMWR Morb Mortal Wkly Rep* 70: 202–207, 2021.

Mellen NM, **Janczewski WA**, **Bocchiaro CM**, **Feldman JL**. Opioid-Induced Quantal Slowing Reveals Dual Networks for Respiratory Rhythm Generation. *Neuron* 37: 821–826, 2003.

Montandon G. Chapter 12 - The pathophysiology of opioid-induced respiratory depression. In: *Handbook of Clinical Neurology*, edited by Chen R, Guyenet PG. Elsevier, p. 339–355.

Montandon G, **Liu H**, **Horner RL**. Contribution of the respiratory network to rhythm and motor output revealed by modulation of GIRK channels, somatostatin and neurokinin-1 receptors. *Sci Rep* 6: 32707, 2016a.

Montandon G, **Ren J**, **Victoria NC**, **Liu H**, **Wickman K**, **Greer JJ**, **Horner RL**. G-protein–gated Inwardly Rectifying Potassium Channels Modulate Respiratory Depression by Opioids. *Anesthesiology* 124: 641–650, 2016b.

Nectow AR, **Nestler EJ**. Viral tools for neuroscience. *Nat Rev Neurosci* 21: 669–681, 2020.

Neumueller SE, **Buiter N**, **Hilbert G**, **Grams K**, **Taylor R**, **Desalvo J**, **Hodges GL**, **Hodges MM**, **Pan LG**, **Lewis SJ**, **Forster HV**, **Hodges MR**. Effects of sub-lethal doses of fentanyl on vital physiologic functions and withdrawal-like behaviors in adult goats. *Front Physiol* 14, 2023.

O'Connor R, **Segers LS**, **Morris KF**, **Nuding SC**, **Pitts T**, **Bolser DC**, **Davenport PW**, **Lindsey BG**. A Joint Computational Respiratory Neural Network-Biomechanical Model for Breathing and Airway Defensive Behaviors. *Front Physiol* 3, 2012.

Palkovic B, **Marchenko V**, **Zuperku EJ**, **Stuth EAE**, **Stucke AG**. Multi-Level Regulation of Opioid-Induced Respiratory Depression. *Physiology* 35: 391–404, 2020.

Pattinson KTS. Opioids and the control of respiration. *Br J Anaesth* 100: 747–758, 2008.

Phillips RS, **Baertsch NA**. Interdependence of cellular and network properties in respiratory rhythm generation. *Proc Natl Acad Sci* 121: e2318757121, 2024.

Ramirez J-M, **Burgraff NJ**, **Wei AD**, **Baertsch NA**, **Varga AG**, **Baghdoyan HA**, **Lydic R**, **Morris KF**, **Bolser DC**, **Levitt ES**. Neuronal mechanisms underlying opioid-induced respiratory depression: our current understanding. *J Neurophysiol* 125: 1899–1919, 2021.

Segers LS, **Nuding SC**, **Dick TE**, **Shannon R**, **Baekey DM**, **Solomon IC**, **Morris KF**, **Lindsey BG**. Functional connectivity in the pontomedullary respiratory network. *J Neurophysiol* 100: 1749–1769, 2008.

Segers LS, **Nuding SC**, **Ott MM**, **Dean JB**, **Bolser DC**, **O'Connor R**, **Morris KF**, **Lindsey BG**. Peripheral chemoreceptors tune inspiratory drive via tonic expiratory neuron hubs in the medullary ventral respiratory column network. *J Neurophysiol* 113: 352–368, 2015.

Shen TY, **Poliacek I**, **Rose MJ**, **Musselwhite MN**, **Kotmanova Z**, **Martvon L**, **Pitts T**, **Davenport PW**, **Bolser DC**. The role of neuronal excitation and inhibition in the pre-Bötzinger complex on the cough reflex in the cat. *J Neurophysiol* 127: 267–278, 2022.

Shevtsova NA, **Manzke T**, **Molkov YI**, **Bischoff A**, **Smith JC**, **Rybak IA**, **Richter DW**. Computational modelling of 5-HT receptor-mediated reorganization of the brainstem respiratory network. *Eur J Neurosci* 34: 1276–1291, 2011.

da Silva CA, **Grover CJ**, **Picardo MCD**, **Del Negro CA**. Role of NaV1.6-mediated persistent sodium current and bursting-pacemaker properties in breathing rhythm generation. *Cell Rep* 42: 113000, 2023.

Simera M, **Poliacek I**, **Jakus J**. Central antitussive effect of codeine in the anesthetized rabbit. *Eur J Med Res* 15: 184, 2010.

Skulsky EM, **Osman NI**, **Baghdoyan HA**, **Lydic R**. Microdialysis Delivery of Morphine to the Hypoglossal Nucleus of Wistar Rat Increases Hypoglossal Acetylcholine Release. *Sleep* 30: 566–573, 2007.

Song C, **Alijani A**, **Frank T**, **Hanna GB**, **Cuschieri A**. Mechanical properties of the human abdominal wall measured in vivo during insufflation for laparoscopic surgery. *Surg Endosc* 20: 987–990, 2006.

715 **Sun X**, **Thörn Pérez C**, **Halemani D N**, **Shao XM**, **Greenwood M**, **Heath S**, **Feldman JL**, **Kam K**. Opioids modulate
716 an emergent rhythmogenic process to depress breathing. *eLife* 8: e50613, 2019.
717 **Sutter ME**, **Wintemute GJ**, **Clarke SO**, **Roche BM**, **Chenoweth JA**, **Gutierrez R**, **Albertson TE**. The Changing Use of
718 Intravenous Opioids in an Emergency Department. *West J Emerg Med* 16: 1079, 2015.
719 **Tomazini Martins R**, **Carberry JC**, **Gandevia SC**, **Butler JE**, **Eckert DJ**. Effects of morphine on respiratory load
720 detection, load magnitude perception, and tactile sensation in obstructive sleep apnea. *J Appl Physiol* 125:
721 393–400, 2018.
722 **Varga AG**, **Reid BT**, **Kieffer BL**, **Levitt ES**. Differential impact of two critical respiratory centres in opioid-induced
723 respiratory depression in awake mice. *J Physiol* 598: 189–205, 2019.
724 **Varga AG**, **Reid BT**, **Kieffer BL**, **Levitt ES**. Differential impact of two critical respiratory centres in opioid-induced
725 respiratory depression in awake mice. *J Physiol* 598: 189–205, 2020.
726 **Wenninger JM**, **Pan LG**, **Klum L**, **Leekley T**, **Bastastic J**, **Hodges MR**, **Feroah TR**, **Davis S**, **Forster HV**. Large lesions
727 in the pre-Bötzinger complex area eliminate eupneic respiratory rhythm in awake goats. *J Appl Physiol* 97:
728 1629–1636, 2004.
729 **Wolf SJ**, **Byyny R**, **Carpenter CR**, **Diercks DB**, **Gemme SR**, **Gerardo CJ**, **Godwin SA**, **Hahn SA**, **Hatten BW**, **Haukoos**
730 **JS**, **Hickey SM**, **Kaji A**, **Kwok H**, **Lo BM**, **Mace SE**, **Nazarian DJ**, **Promes SB**, **Shah KH**, **Shih RD**, **Silvers SM**,
731 **Smith MD**, **Thiessen MEW**, **Tomaszewski CA**, **Valente JH**, **Wall SP**, **Winger J**, **Cantrill SV**, **Hirshon JM**, **Mims**
732 **M**, **Schulz T**, **Hatten BW**, **Cantrill SV**, **Dubin JS**, **Ketcham EM**, **Runde DP**, **Wall SP**, **Wolf SJ**. Clinical Policy:
733 Critical Issues Related to Opioids in Adult Patients Presenting to the Emergency Department. *Ann Emerg*
734 *Med* 76: e13–e39, 2020.

735

736

737

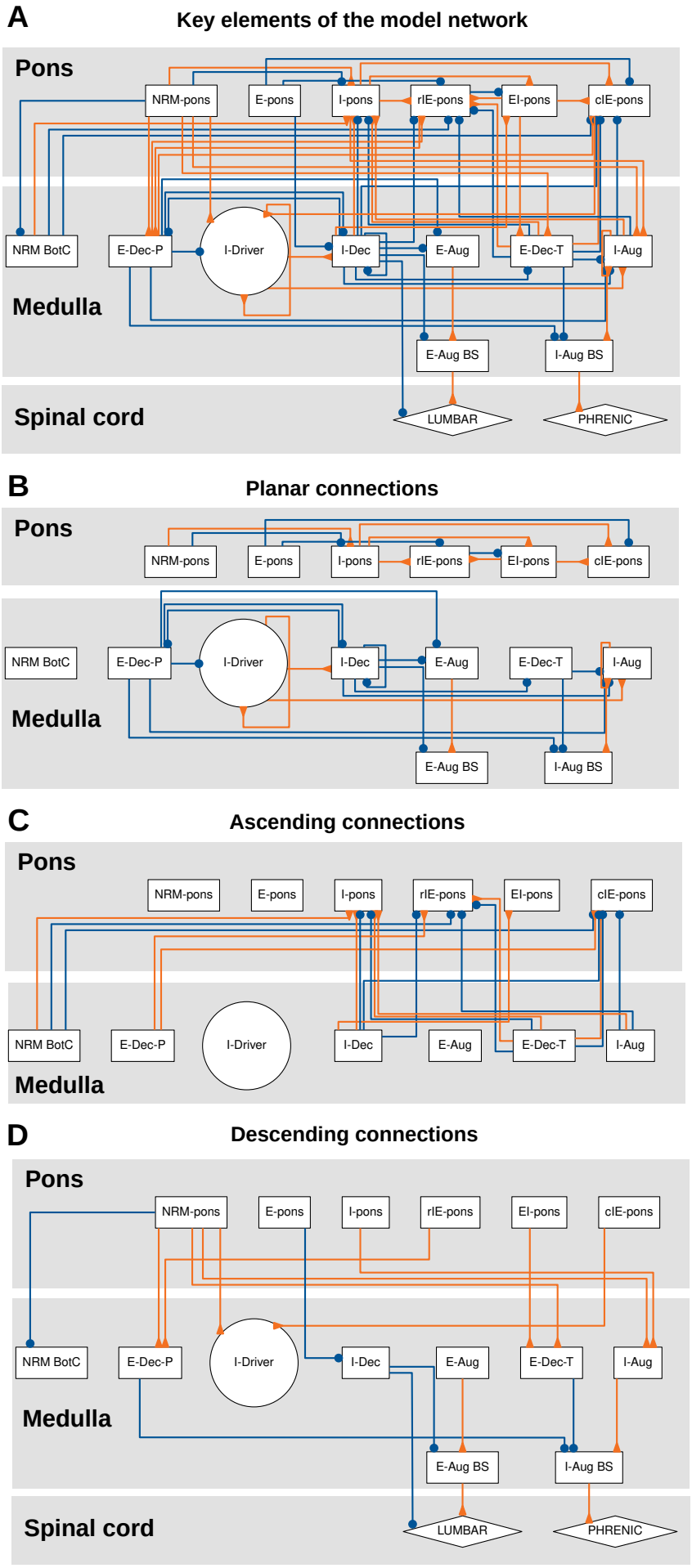
A
Key elements of the model network
Pons
NRM-pons
E-pons
I-pons
rIE-pons
EI-pons
cIE-pons
NRM BotC
E-Dec-P
I-Driver
I-Dec
E-Aug
E-Dec-T
I-Aug
Medulla
E-Aug BS
I-Aug BS
Spinal cord
LUMBAR
PHRENIC
B
Planar connections
Pons
NRM-pons
E-pons
I-pons
rIE-pons
EI-pons
cIE-pons
NRM BotC
E-Dec-P
I-Driver
I-Dec
E-Aug
E-Dec-T
I-Aug
Medulla
E-Aug BS
I-Aug BS
C
Ascending connections
Pons
NRM-pons
E-pons
I-pons
rIE-pons
EI-pons
cIE-pons
NRM BotC
E-Dec-P
I-Driver
I-Dec
E-Aug
E-Dec-T
I-Aug
Medulla
D
Descending connections
Pons
NRM-pons
E-pons
I-pons
rIE-pons
EI-pons
cIE-pons
NRM BotC
E-Dec-P
I-Driver
I-Dec
E-Aug
E-Dec-T
I-Aug
Medulla
E-Aug BS
I-Aug BS
Spinal cord
LUMBAR
PHRENIC

Figure 1

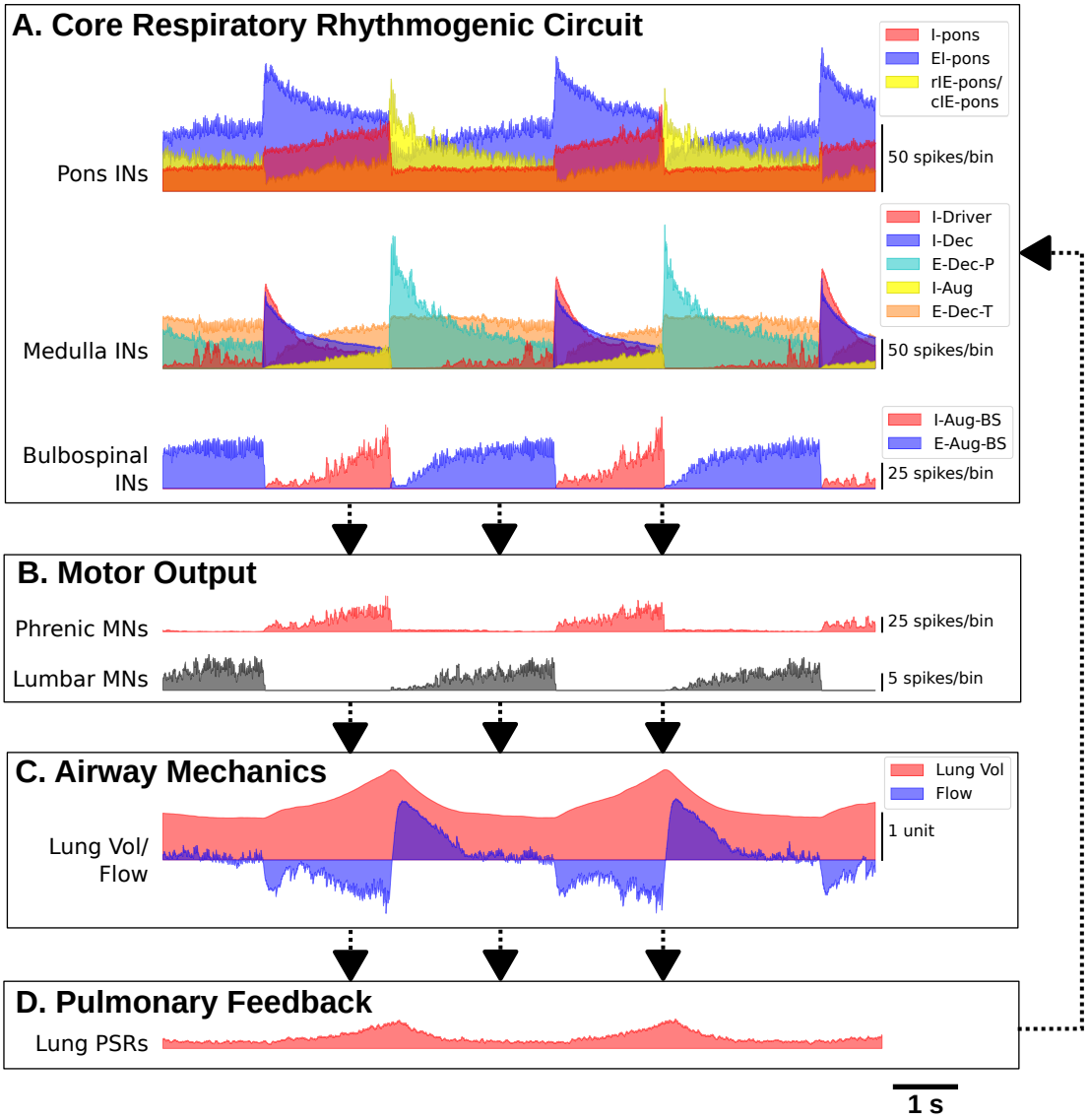
A. Core Respiratory Rhythmogenic Circuit
I-pons
EI-pons
rIE-pons/
cIE-pons
Pons INs
50 spikes/bin
I-Driver
I-Dec
E-Dec-P
I-Aug
E-Dec-T
Medulla INs
50 spikes/bin
I-Aug-BS
E-Aug-BS
Bulbospinal
INs
25 spikes/bin
B. Motor Output
Phrenic MNs
25 spikes/bin
Lumbar MNs
5 spikes/bin
C. Airway Mechanics
Lung Vol
Flow
Lung Vol/
Flow
1 unit
D. Pulmonary Feedback
Lung PSRs
1 s

Figure 2

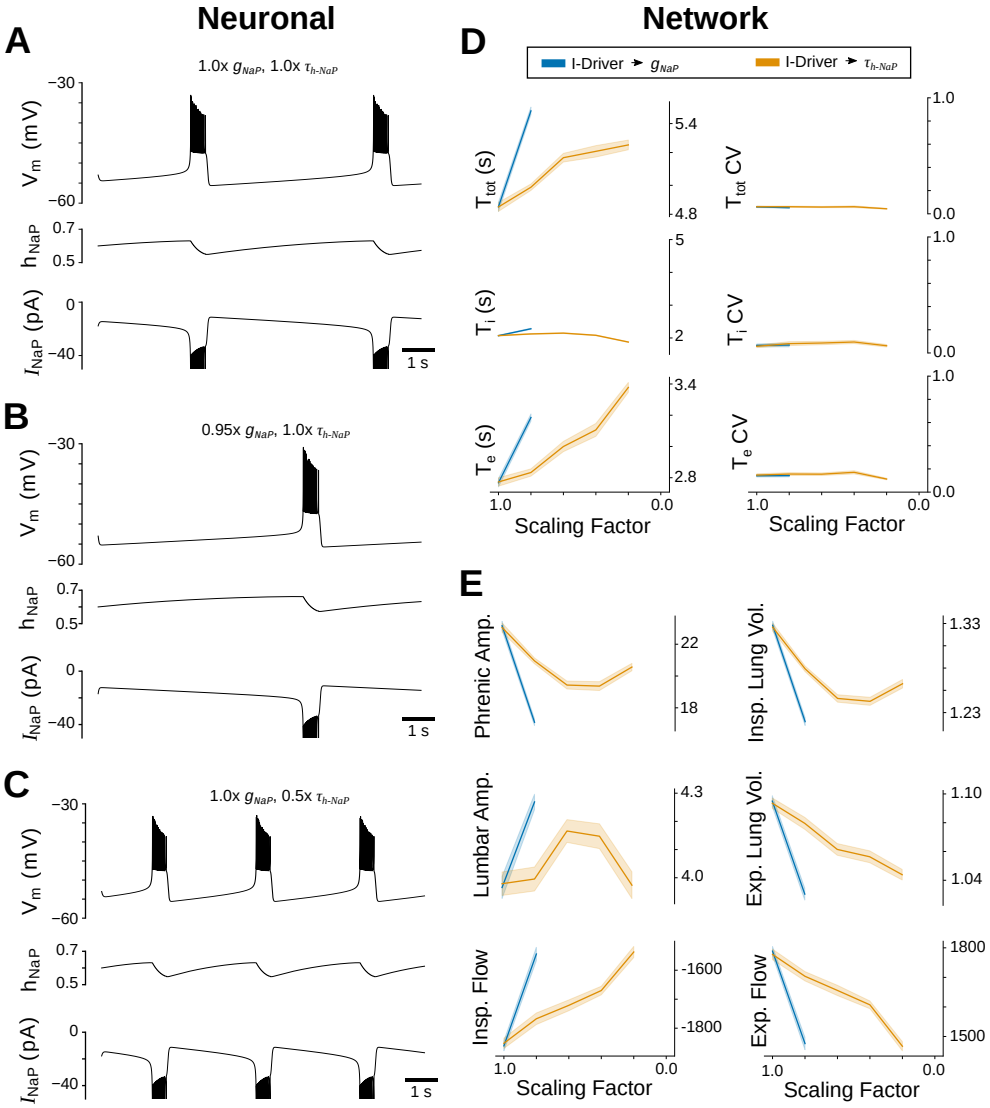
Neuronal
Network
A
1.0x g_{NaP}, 1.0x $\tau_{h\text{-}NaP}$
B
0.95x g_{NaP}, 1.0x $\tau_{h\text{-}NaP}$
C
1.0x g_{NaP}, 0.5x $\tau_{h\text{-}NaP}$
V_m (mV)
h_{NaP}
I_{NaP} (pA)
1 s
D
I-Driver → g_{NaP}
I-Driver → $\tau_{h\text{-}NaP}$
T_{tot} (s)
T_{tot} CV
T_i (s)
T_i CV
T_e (s)
T_e CV
Scaling Factor
E
Phrenic Amp.
Insp. Lung Vol.
Lumbar Amp.
Exp. Lung Vol.
Insp. Flow
Exp. Flow

Figure 3

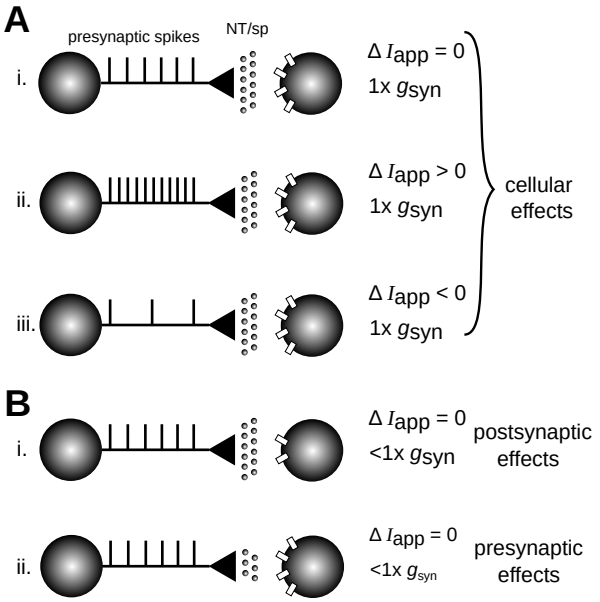
A
presynaptic spikes
NT/sp
i.
Δ I_{app} = 0
1x g_{syn}
ii.
Δ I_{app} > 0
1x g_{syn}
iii.
Δ I_{app} < 0
1x g_{syn}
cellular effects
B
i.
Δ I_{app} = 0
<1x g_{syn}
postsynaptic effects
ii.
Δ I_{app} = 0
<1x g_{syn}
presynaptic effects

Figure 4

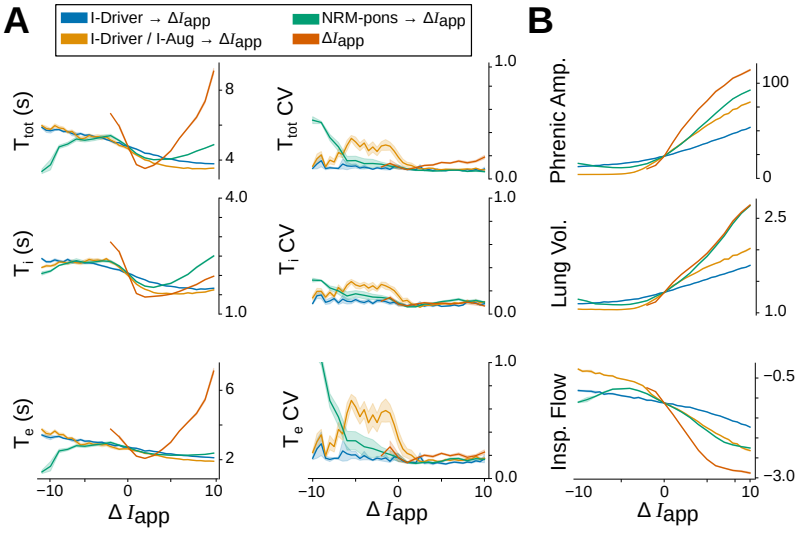
A
I-Driver → ΔIapp
I-Driver / I-Aug → ΔIapp
NRM-pons → ΔIapp
ΔIapp
B
Ttot (s)
Ti (s)
Te (s)
Ttot CV
Ti CV
Te CV
Phrenic Amp.
Lung Vol.
Insp. Flow
Δ Iapp

Figure 5

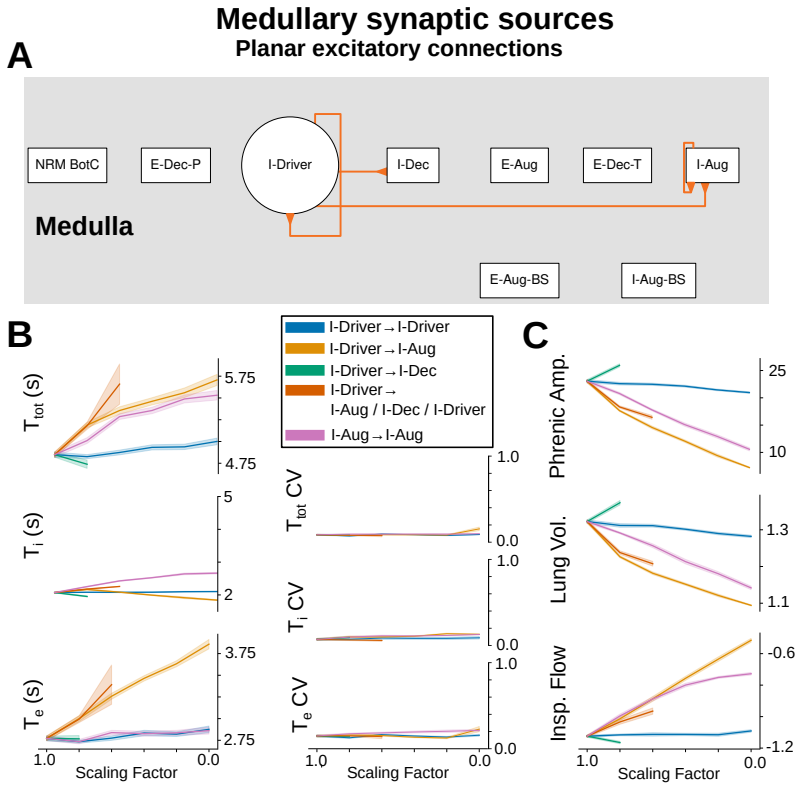
Medullary synaptic sources
Planar excitatory connections
A
NRM BotC
E-Dec-P
I-Driver
I-Dec
E-Aug
E-Dec-T
I-Aug
Medulla
E-Aug-BS
I-Aug-BS
B
I-Driver→I-Driver
I-Driver→I-Aug
I-Driver→I-Dec
I-Driver→
I-Aug / I-Dec / I-Driver
I-Aug→I-Aug
C
Ttot (s)
Ti (s)
Te (s)
Ttot CV
Ti CV
Te CV
Phrenic Amp.
Lung Vol.
Insp. Flow
Scaling Factor

Figure 6

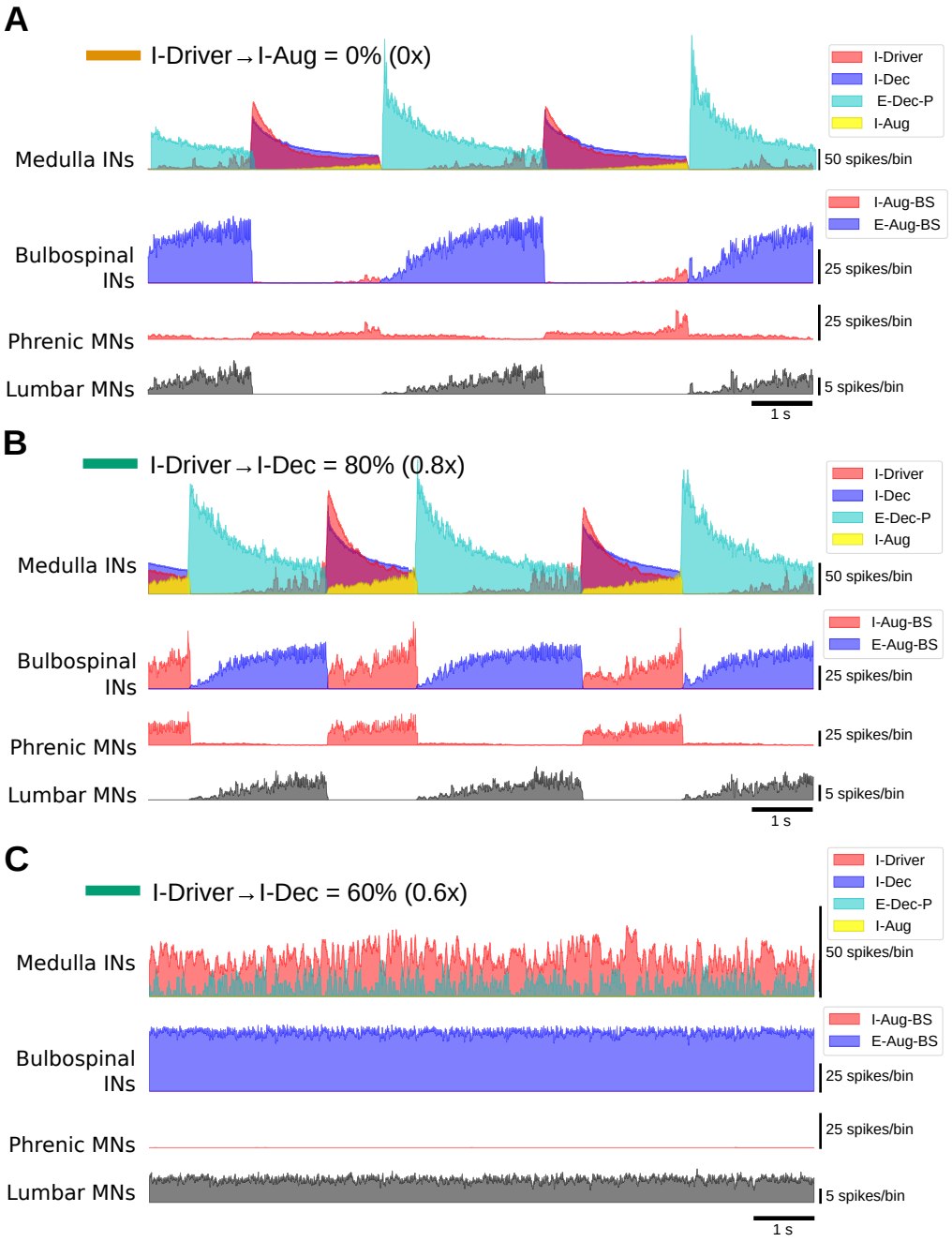
A
I-Driver → I-Aug = 0% (0x)
I-Driver
I-Dec
E-Dec-P
I-Aug
Medulla INs
50 spikes/bin
I-Aug-BS
E-Aug-BS
Bulbospinal INs
25 spikes/bin
Phrenic MNs
25 spikes/bin
Lumbar MNs
5 spikes/bin
1 s
B
I-Driver → I-Dec = 80% (0.8x)
I-Driver
I-Dec
E-Dec-P
I-Aug
Medulla INs
50 spikes/bin
I-Aug-BS
E-Aug-BS
Bulbospinal INs
25 spikes/bin
Phrenic MNs
25 spikes/bin
Lumbar MNs
5 spikes/bin
1 s
C
I-Driver → I-Dec = 60% (0.6x)
I-Driver
I-Dec
E-Dec-P
I-Aug
Medulla INs
50 spikes/bin
I-Aug-BS
E-Aug-BS
Bulbospinal INs
25 spikes/bin
Phrenic MNs
25 spikes/bin
Lumbar MNs
5 spikes/bin
1 s

Figure 7

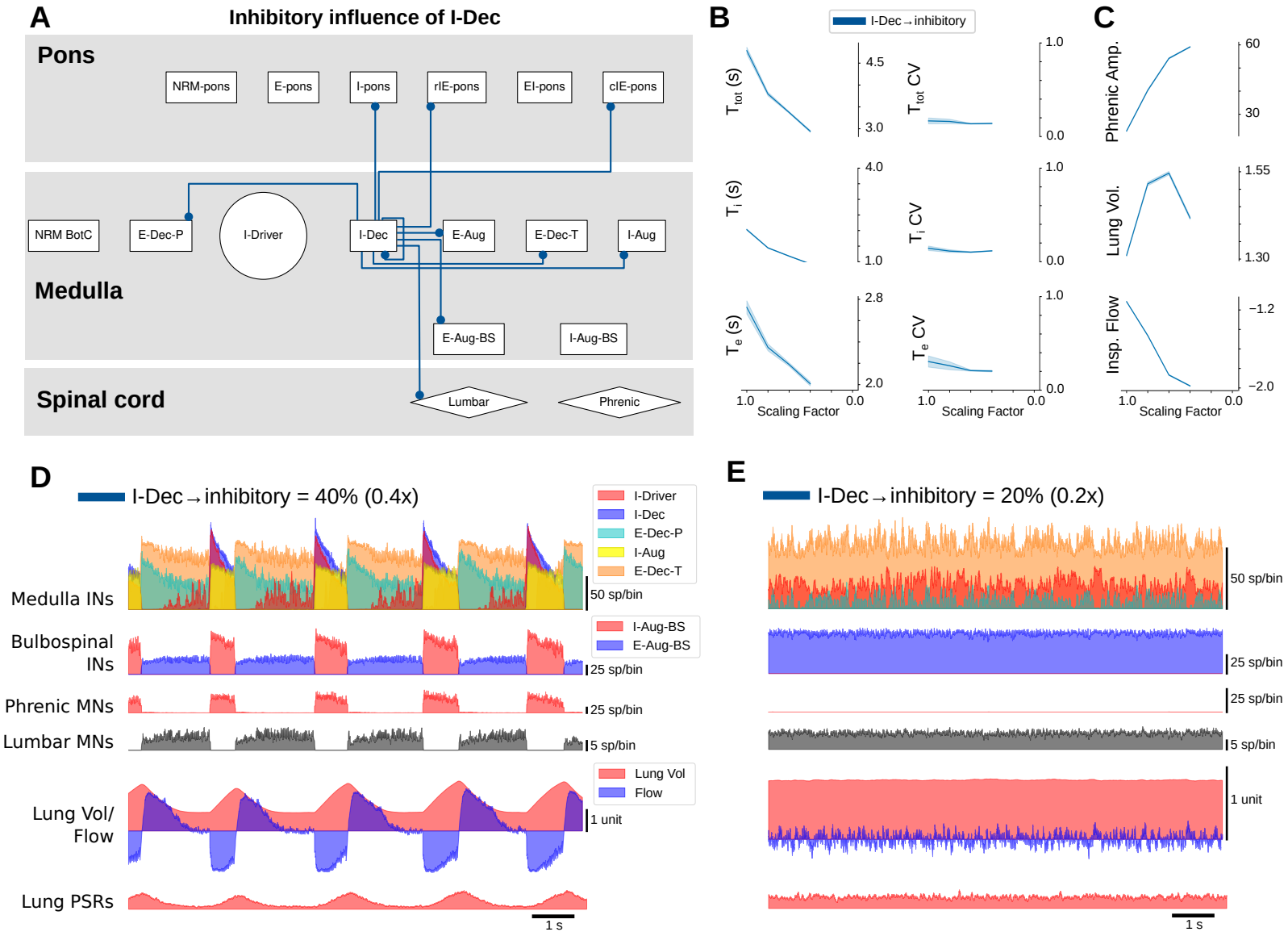
A
Inhibitory influence of I-Dec
Pons
NRM-pons
E-pons
I-pons
rIE-pons
EI-pons
cIE-pons
NRM BotC
E-Dec-P
I-Driver
I-Dec
E-Aug
E-Dec-T
I-Aug
Medulla
E-Aug-BS
I-Aug-BS
Spinal cord
Lumbar
Phrenic
B
I-Dec→inhibitory
T_tot (s)
T_tot CV
T_i (s)
T_i CV
T_e (s)
T_e CV
Scaling Factor
C
Phrenic Amp.
Lung Vol.
Insp. Flow
Scaling Factor
D
I-Dec→inhibitory = 40% (0.4x)
I-Driver
I-Dec
E-Dec-P
I-Aug
E-Dec-T
Medulla INs
50 sp/bin
I-Aug-BS
E-Aug-BS
Bulbospinal INs
25 sp/bin
Phrenic MNs
25 sp/bin
Lumbar MNs
5 sp/bin
Lung Vol
Flow
Lung Vol/ Flow
1 unit
Lung PSRs
1 s
E
I-Dec→inhibitory = 20% (0.2x)
50 sp/bin
25 sp/bin
25 sp/bin
5 sp/bin
1 unit
1 s

Figure 8

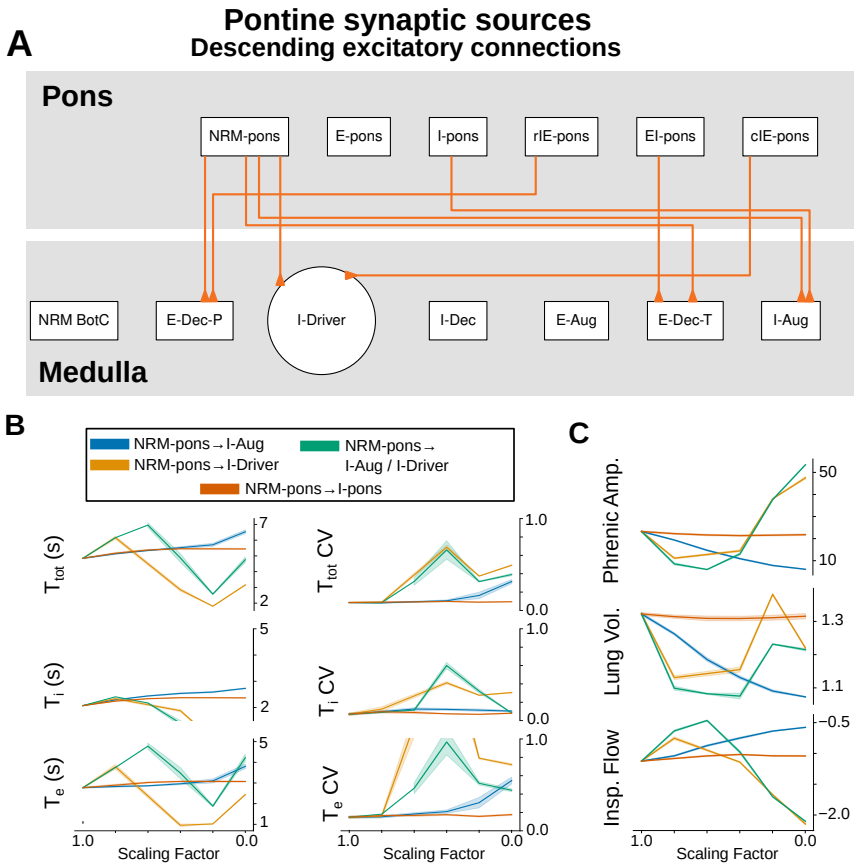
A
Pontine synaptic sources
Descending excitatory connections
Pons
NRM-pons
E-pons
I-pons
rIE-pons
EI-pons
cIE-pons
NRM BotC
E-Dec-P
I-Driver
I-Dec
E-Aug
E-Dec-T
I-Aug
Medulla
B
NRM-pons→I-Aug
NRM-pons→I-Driver
NRM-pons→I-Aug / I-Driver
NRM-pons→I-pons
T_tot (s)
T_i (s)
T_e (s)
T_tot CV
T_i CV
T_e CV
Scaling Factor
C
Phrenic Amp.
Lung Vol.
Insp. Flow
Scaling Factor

Figure 9

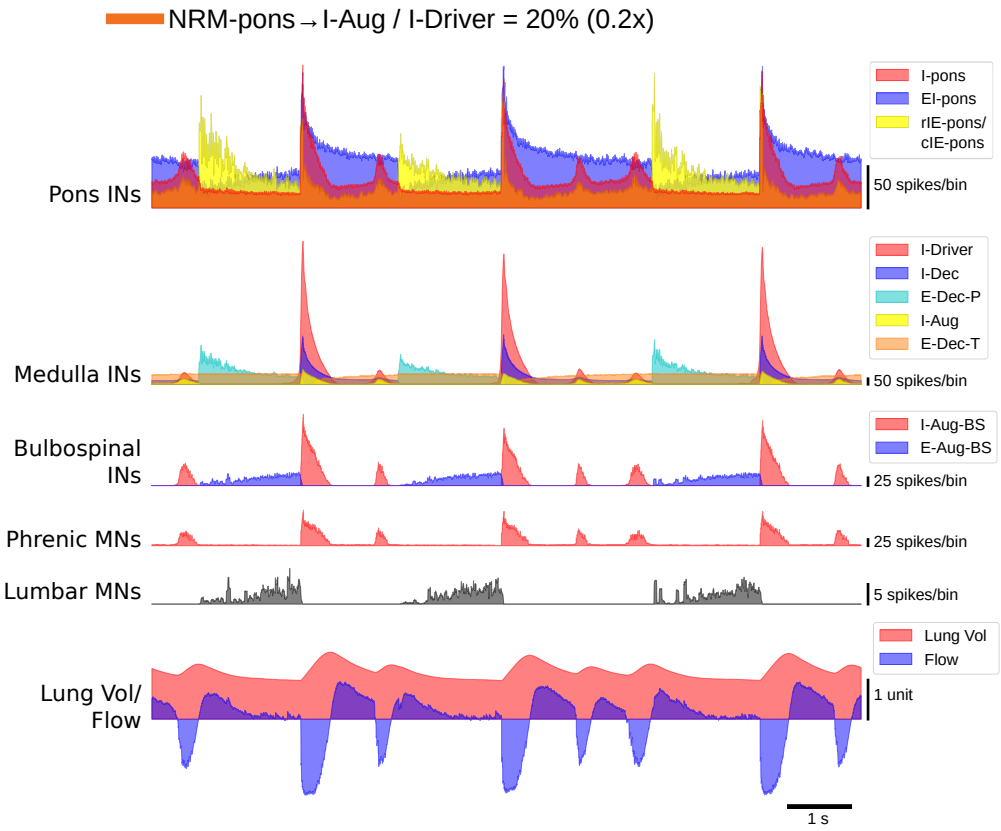
NRM-pons→I-Aug / I-Driver = 20% (0.2x)
Pons INs
I-pons
EI-pons
rIE-pons/
cIE-pons
50 spikes/bin
Medulla INs
I-Driver
I-Dec
E-Dec-P
I-Aug
E-Dec-T
50 spikes/bin
Bulbospinal
INs
I-Aug-BS
E-Aug-BS
25 spikes/bin
Phrenic MNs
25 spikes/bin
Lumbar MNs
5 spikes/bin
Lung Vol/
Flow
Lung Vol
Flow
1 unit
1 s

Figure 10